PRESENTATION AND INTERPRETATION OF GRAVITY AND MAGNETIC DATA IN THE PORCUPINE BASIN

PSG Project P00/4

Prepared for
Porcupine Studies Group
Petroleum Infrastructure Programme Group 3

Prepared by
PGW Europe Ltd.

103B Rathgar Road
Dublin, Ireland
tel: + 353 1 4929456
fax: + 353 1 4929458
email: tomdavitt@eircom.net
web: www.pgw.on.ca

March, 2001 Dublin, Ireland

Table of Contents

List of Figures

Acknowledgements

This Project, including data and survey results acquired for the purpose, has been undertaken on behalf of the Porcupine Studies Group (PSG) of the Petroleum Infrastructure Programme Group 3 which was established by the Petroleum Affairs Division of the Department of the Marine and Natural Resources on 15 March 1999 in conjunction with the award of exploration licences under the South Porcupine Licensing Round. The PSG comprises: Agip Ireland BV, Chevron UK Ltd, Elf Petroleum Ireland BV, Enterprise Energy Ireland Ltd, Marathon International Hibernia Ltd, Phillips Petroleum Company United Kingdom Ltd, Statoil Exploration (Ireland) Ltd and the Petroleum Affairs Division of the Department of the Marine and Natural Resources.

1. Introduction

In October 2000, PGW Europe Ltd. was contracted by PIPCo RSG Ltd. to undertake Phase 2 of a three-phase project concerning the Compilation, Presentation and Interpretation of Gravity and Magnetic Data in the Porcupine Basin. Phase 1, consisting of the compilation of the gravity and magnetic data, was undertaken by ARK Geophysics Ltd. of Milton Keynes, United Kingdom (ARK Geophysics Ltd., 2000). This report concerns Phase 2, consisting of the presentation and interpretation of the data. The study area is bounded by 15º 00´ W, 8º 00´ W, 48º 27´ N and 53º 37´ N. The actual data coverage and interpretation has been extended another 50 km or so beyond these boundaries. A CD accompanies this report, containing the thirty-one maps described in chapter 3 in several digital forms, as well as the grids and databases used to prepare these maps.

2. Data Sources and Compilation

The report on Phase 1 of this project (ARK Geophysics Ltd., 2000) describes the datasets that were compiled and merged to provide the basic grids of gravity and magnetic data used to prepare the products for Phase 2.

The following datasets were utilized in the gravity compilation (Figure 1):

Source	Dataset
Petroleum Affairs Division (P.A.D)	Offshore free air gravity
D.T. Sandwell's Geosat and ERS.1 satellite altimeter profile	Offshore free air gravity

Dublin Institute for Advanced Studies (D.I.A.S)	Onshore Bouguer gravity

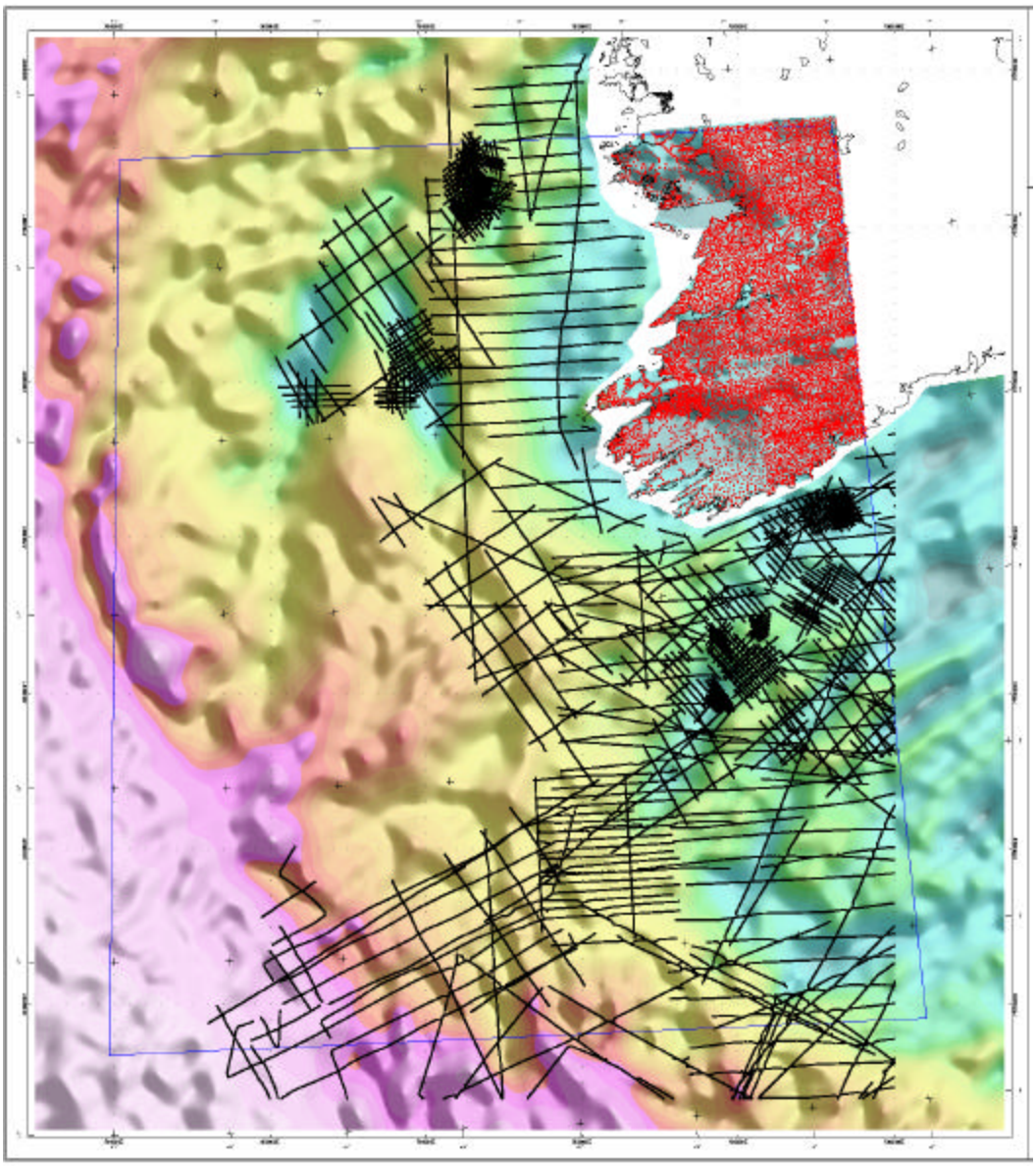

Figure 1 *Gravity data coverage superimposed on Bouguer gravity image shaded from the northeast. Land gravity stations (D.I.A.S.) shown in red. Gravity ship tracks (P.A.D.) shown in black (missing east of 1 000 000 E). Area to west lacking coverage utilizes the satellite altimeter data (Sandwell).*

The following datasets were utilized in the magnetic compilation (Figure 2):

Source	Dataset
Petroleum Affairs Division (P.A.D)	Offshore aeromagnetic database

Enterprise Oil PLC	Integrated aeromagnetic compilation comprised of the following datasets: Chevron 1995 North Porcupine Basin Texaco 1995 South Slyne Trough NOPEC-Geoventures 1997 South Porcupine Basin
Geological Survey of Ireland (G.S.I)	Onshore aeromagnetics

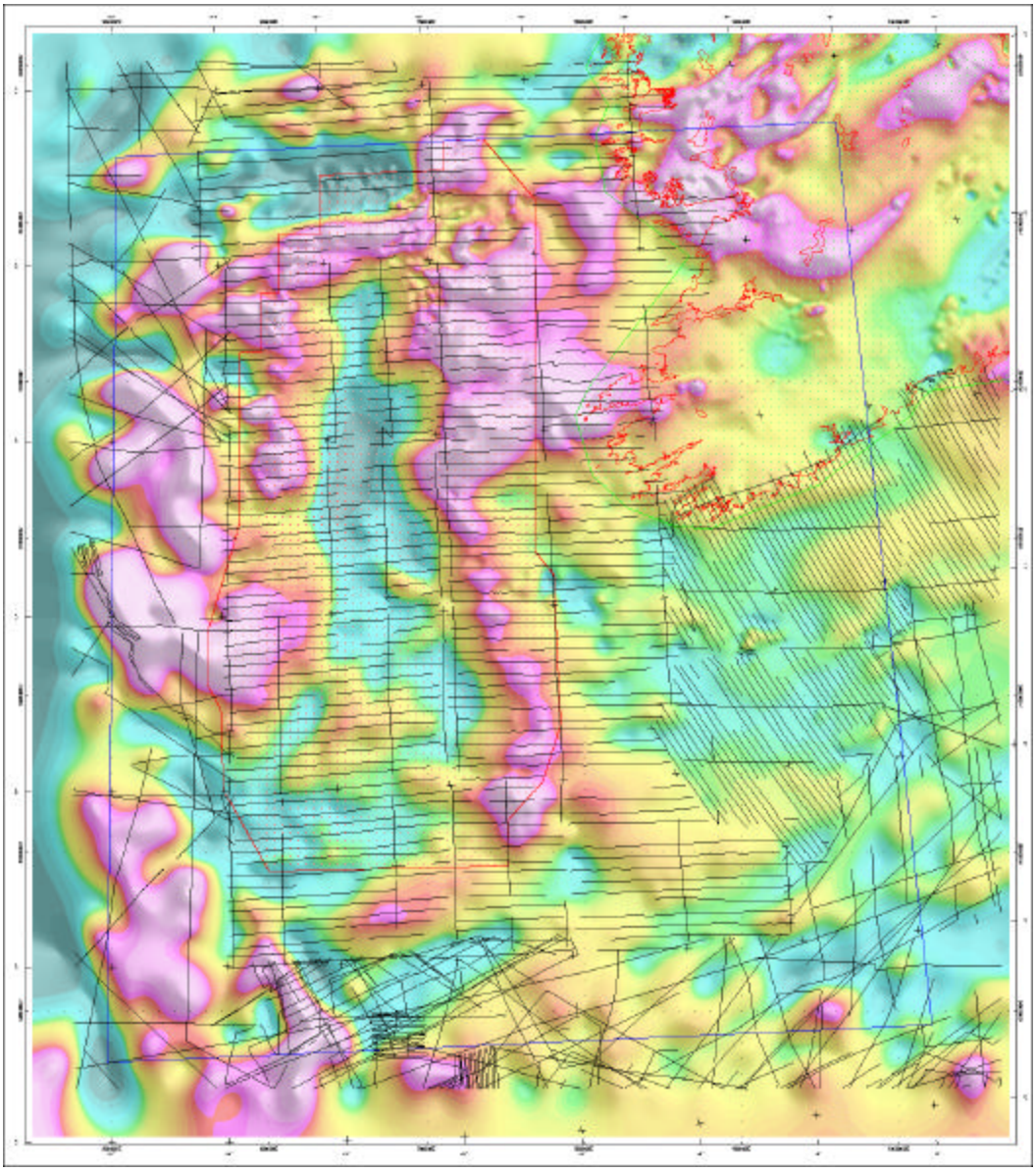

Figure 2 *Magnetic data coverage superimposed on magnetic anomaly image (excludes high-resolution offshore survey) shaded from the northeast. Offshore aeromagnetic flightlines (P.A.D.) shown in black. Offshore high-resolution aeromagnetic grid shown in red. Onshore aeromagnetic grid (G.S.I.) shown in green.*

Two versions of the magnetic products were prepared, one with and the other without the NOPEC-Geoventures 1997 South Porcupine Basin survey. This was to accommodate PSG members who either had or had not purchased the rights to those data.

The following digital products, originally prepared by ARK Geophysics Ltd., were provided to PGW Europe Ltd. to undertake Phase 2:

1) Topography / bathymetry grid;
2) Free air gravity grid;
3) Bouguer gravity grid;
4) Magnetic anomaly grid;
5) X-Y coordinates of gravity stations, gravity shiptracks, aeromagnetic flightlines and aeromagnetic compilation grids; and
6) Compilation report.

The data were prepared by ARK Geophysics Ltd. in the coordinate system described below, and which was also used for all digital and map products in Phase 2:

Projection: Universal Transverse Mercator
Spheroid: International 1924 (Hayford)
Geodetic Datum: ED50
Central Meridian: 15º00´ W
Latitude of origin: 0º00´ N
False Easting: 500000 m
False Northing: 0 m
Scale Factor: 0.9996
Semimajor Axis: 6378388.0 m
Semiminor Axis: 6356911.9 m

3. Data Processing and Map Preparation

PGW Europe Ltd. prepared a series of map products, with associated grids and databases, as described below. All of the data processing and map production was undertaken using Geosoft's OASIS montaj™, with the exception of the interpretation map which was drafted using AutoCAD 2000™. The original work order required twenty-three map products (Maps 1 to 23). These were supplemented by an additional eight map products proposed by PGW Europe Ltd. (Maps 20-2, 21-2 and 24 to 29). The magnetic maps were prepared in two versions, with and without the NOPEC-Geoventures 1997 South Porcupine Basin survey.

The digital data have been exported from Geosoft to a variety of formats, to accommodate the PSG members.

Map 1 – Magnetic and Gravity Interpretation

See section 4 for a discussion of the interpretation map.

Map 2 - Bathymetry Image With Contours

The bathymetry-topography grid was resampled to a pitch of 1 km. Colour break levels are set at variable intervals as modified from on equal-area colour distribution. Annotated contours use a base interval of 10 metres between –200m to 0m, and 20 metres for the rest.

The bathymetry image is useful for correlating geomorphologic features with the geophysical data and for incorporation in interpretation.

Map 3 – Gravity Data Distribution

The gravity data distribution was prepared as shown in Figure 1 (without the gravity image). No shiptracks were provided to PGW Europe Ltd. for the southeastern portion of the map area. The satellite altimeter data was used to fill the blank area to the west.

There is a gap in the gravity coverage along the Irish coast. There are no marine data available for this area, and satellite gravity data cannot be used, as they are unreliable in coastal areas. During Phase I of this project (ARK Geophysics Ltd., 2000), attempts were made to spline across this gap but they were ultimately unsuccessful.

Map 4 – Magnetic Data Distribution

The magnetic data distribution was prepared as shown in Figure 2 (without the magnetic image). The flightpath for the onshore and high-resolution offshore surveys were not provided to PGW Europe Ltd.

Map 5 - Free Air Gravity Anomaly Image With Shaded Relief

The free air gravity anomaly grid is presented without additional treatment. Colour break levels are set at variable intervals as modified from an equal-area colour distribution. Shaded relief illumination is applied from the north at a 45º inclination to the horizon. Bouguer gravity data is used for the onshore area.

Map 6 - Horizontal Gradient of the Free Air Gravity Anomaly Image With Shaded Relief

The grid of the horizontal gradient of the free air gravity anomaly was prepared by computing the gradient amplitude as $[(dF/dx)^2 + (dF/dy)^2]^{1/2}$ in the space-domain. Colour break levels are set at variable

intervals as modified from an equal-area colour distribution. Shaded relief illumination is applied from the north at a 45º inclination to the horizon.

Map 7 - Residual of the Free Air Gravity Anomaly Image With Shaded Relief

The grid of the residual of the free air gravity anomaly was prepared by computing the free air gravity anomaly upward continued 10 km, in the frequency-domain, and subtracting it from the original free air gravity. Colour break levels are set at variable intervals as modified from an equal-area colour distribution. Shaded relief illumination is applied from the north at a 45º inclination to the horizon.

Map 8 - Isostatically-corrected Bouguer Gravity Anomaly Image With Shaded Relief

The Bouguer gravity anomaly was isostatically corrected by computing the isostatic effect assuming a crustal thickness of 40 km, Bouguer densities of 2.67 gm/cc and 2.20 gm/cc for onshore and offshore respectively, and mantle density of 3.27 gm/cc. These parameters were determined using the method of Chapin (1996). Based on this model, the isostatic regional grid was calculated, utilising a GX from Northwest Geophysical Associates, and subtracted from the Bouguer gravity grid. Colour break levels are set at variable intervals as modified from an equal-area colour distribution. Shaded relief illumination is applied from the north at a 45º inclination to the horizon.

Map 9 - Horizontal Gradient of the Isostatically-corrected Bouguer Gravity Anomaly Image With Shaded Relief

The grid of the horizontal gradient of the isostatically-corrected Bouguer gravity anomaly was prepared by computing the gradient amplitude as $[(dF/dx)^2 + (dF/dy)^2]^{1/2}$. Colour break levels are set at variable intervals as modified from an equal-area colour distribution. Shaded relief illumination is applied from the north at a 45º inclination to the horizon.

Map 10 - Residual of the Isostatically-corrected Bouguer Gravity Anomaly Image With Shaded Relief

The grid of the residual of the isostatically-corrected Bouguer gravity anomaly was prepared by computing the isostatically-corrected Bouguer gravity anomaly upward continued 10 km, in the frequency-domain, and subtracting it from the original isostatically-corrected Bouguer gravity. Colour break levels are set at variable intervals as modified from an equal-area colour distribution. Shaded relief illumination is applied from the north at a 45º inclination to the horizon.

Map 11 - Gravity Euler Solutions for a Structural Index of 0.0

Euler deconvolution (Reid et al, 1990) was applied to the grid of the isostatically-corrected Bouguer gravity anomaly. The parameters used were as follows:

Structural index – 0.0 (sill/dyke/step model)
Window size – 10 km x 10 km
Maximum vertical uncertainty – 15%
Maximum horizontal uncertainty – 30%

Solutions above ground surface have been omitted. Solutions below 40 km below surface have been set to 40 km below surface for presentation purposes. The solutions are presented as circles with colour scaled to depth below ground/sea surface, with colour break levels set at variable intervals as modified from an equal-area colour distribution. The circle diameters are also scaled to reflect depth (4000m/mm).

Map 12 - Total Magnetic Field Anomaly Image With Contours

The total magnetic field anomaly grid is presented without additional treatment. Colour break levels are set at variable intervals as modified from an equal-area colour distribution. Annotated contours use a base interval of 5 nanoteslas.

Map 13 - Reduction-to-the-Pole of the Total Magnetic Field Anomaly Image With Shaded Relief

The grid of the reduction-to-the-pole of the total magnetic field anomaly was prepared by applying a pole-reduction filter in the frequency-domain. Colour break levels are set at variable intervals as modified from an equal-area colour distribution. Shaded relief illumination is applied from the north at a 45º inclination to the horizon.

Map 14 - Reduction-to-the-Pole of the Total Magnetic Field Anomaly Image Shaded from the North

The grid of the reduction-to-the-pole of the total magnetic field anomaly was prepared by applying a pole-reduction filter in the frequency-domain. Shaded relief illumination is applied from the north at a 45º inclination to the horizon. Grey-scale break levels for the shaded relief image are set at variable intervals as modified from an equal-area distribution.

Map 15 - Reduction-to-the-Pole of the Total Magnetic Field Anomaly Image Shaded from the West

The grid of the reduction-to-the-pole of the total magnetic field anomaly was prepared by applying a pole-reduction filter in the

frequency-domain. Shaded relief illumination is applied from the west at a 45º inclination to the horizon. Grey-scale break levels for the shaded relief image are set at variable intervals as modified from an equal-area distribution.

Map 16 - Upward Continuation of the Reduction-to-the-Pole of the Total Magnetic Field Anomaly Image With Shaded Relief

The grid of the upward continuation of the reduction-to-the-pole of the total magnetic field anomaly was prepared by computing the reduction-to-the-pole of the total magnetic field anomaly upward continued 2 km, in the frequency-domain. Colour break levels are set at variable intervals as modified from an equal-area colour distribution. Shaded relief illumination is applied from the north at a 45º inclination to the horizon.

Map 17 - Residual of the Reduction-to-the-Pole of the Total Magnetic Field Anomaly Image With Shaded Relief

The grid of the residual of the reduction-to-the-pole of the total magnetic field anomaly was prepared by computing the reduction-to-the-pole of the total magnetic field anomaly upward continued 2 km, in the frequency-domain, and subtracting it from the original reduction-to-the-pole. Colour break levels are set at variable intervals as modified from an equal-area colour distribution. Shaded relief illumination is applied from the north at a 45º inclination to the horizon.

Map 18 - Analytic Signal of the Total Magnetic Field Anomaly Image With Contours

The grid of the analytic signal of the total magnetic field anomaly was prepared by computing the analytic signal amplitude as $[(dF/dx)^2 + (dF/dy)^2 + (dF/dz)^2]^{1/2}$. The two horizontal gradients were computed in the space-domain, and the first vertical derivative in the frequency-domain. Colour break levels are set at variable intervals as modified from an equal-area colour distribution. Annotated contours use a base interval of 0.0005 nanoteslas/metre.

Map 19 - Horizontal Gradient of the Pseudo-gravity of the Total Magnetic Field Anomaly Image With Shaded Relief

The grid of the pseudo-gravity of the total magnetic field anomaly was prepared by applying a pseudo-gravity filter in the frequency-domain. The horizontal gradient amplitude of the pseudo-gravity was then computed as $[(dF/dx)^2 + (dF/dy)^2]^{1/2}$ in the space-domain. Colour break levels are set at variable intervals as modified from an equal-area colour

distribution. Shaded relief illumination is applied from the north at a 45º inclination to the horizon.

Map 20-1 - Magnetic Euler Solutions for a Structural Index of 0.0

Euler deconvolution (Reid et al., 1990) was applied to the grid of the total magnetic field anomaly. The parameters used were as follows:

Structural index – 0.0 (contact model)
Window size – 10 km x 10 km
Maximum vertical uncertainty – 15%
Maximum horizontal uncertainty – 30%

Solutions above ground surface have been omitted. Solutions below 40 km below surface have been set to 40 km below surface for presentation purposes. The solutions are presented as circles with colour scaled to depth below ground/sea surface, with colour break levels set at variable intervals as modified from an equal-area colour distribution. The circle diameters are also scaled to reflect depth (4000m/mm).

Map 20-2 - Magnetic Euler Solutions for a Structural Index of 1.0

Euler deconvolution (Reid et al., 1990) was applied to the grid of the total magnetic field anomaly. The parameters used were as follows:

Structural index – 1.0 (sill/dyke model)
Window size – 10 km x 10 km
Maximum vertical uncertainty – 15%
Maximum horizontal uncertainty – 30%

Solutions above ground surface have been omitted. Solutions below 40 km below surface have been set to 40 km below surface for presentation purposes. The solutions are presented as circles with colour scaled to depth below ground/sea surface, with colour break levels set at variable intervals as modified from an equal-area colour distribution. The circle diameters are also scaled to reflect depth (4000m/mm).

Map 21-1 - Focused Magnetic Euler Solutions for a Structural Index of 0.0

Euler deconvolution (Reid et al., 1990) was applied to the grid of the total magnetic field anomaly. The solutions were focused by reducing the vertical and horizontal uncertainties. The parameters used were as follows:

Structural index – 0.0 (contact model)
Window size – 10 km x 10 km
Maximum vertical uncertainty – 10%
Maximum horizontal uncertainty – 20%
Maximum distance from window centre – 8 km

Solutions above ground surface have been omitted. Solutions below 40 km below surface have been set to 40 km below surface for presentation purposes. The solutions are presented as circles with colour

scaled to depth below ground/sea surface, with colour break levels set at variable intervals as modified from an equal-area colour distribution. The circle diameters are also scaled to reflect depth.

Map 21-2 - Focused Magnetic Euler Solutions for a Structural Index of 1.0

Euler deconvolution (Reid et al., 1990) was applied to the grid of the total magnetic field anomaly. The solutions were focused by reducing the vertical and horizontal uncertainties. The parameters used were as follows:

Structural index – 1.0 (sill/dyke model)
Window size – 10 km x 10 km
Maximum vertical uncertainty – 10%
Maximum horizontal uncertainty – 20%
Maximum distance from window centre – 8 km

Solutions above ground surface have been omitted. Solutions below 40 km below surface have been set to 40 km below surface for presentation purposes. The solutions are presented as circles with colour scaled to depth below ground/sea surface, with colour break levels set at variable intervals as modified from an equal-area colour distribution. The circle diameters are also scaled to reflect depth.

Map 22 - Isostatically-corrected Bouguer Gravity Anomaly Image With Shaded Relief, Over-posted With Contours of the Reduction-to-the-Pole of the Total Magnetic Field Anomaly

The Bouguer gravity anomaly was isostatically corrected by computing the isostatic effect assuming a crustal thickness of 40 km, Bouguer densities of 2.67 gm/cc and 2.20 gm/cc for onshore and offshore respectively, and mantle density of 3.27 gm/cc. These parameters were determined using the method of Chapin (1996). Based on this model, the isostatic regional grid was calculated, utilising a GX from Northwest Geophysical Associates, and subtracted from the Bouguer gravity grid. Colour break levels are set at variable intervals as modified from an equal-area colour distribution. Shaded relief illumination is applied from the north at a 45º inclination to the horizon.

The grid of the reduction-to-the-pole of the total magnetic field anomaly was prepared by applying a pole-reduction filter in the frequency-domain. Annotated contours use a base interval of 5 nanoteslas.

Map 23 - Reduction-to-the-Pole of the Total Magnetic Field Anomaly Image With Shaded Relief, Over-posted With Contours of the Isostatically-corrected Bouguer Gravity Anomaly

The grid of the reduction-to-the-pole of the total magnetic field anomaly was prepared by applying a pole-reduction filter in the frequency-domain. Colour break levels are set at variable intervals as modified from an equal-area colour distribution. Shaded relief illumination is applied from the north at a 45º inclination to the horizon.

The Bouguer gravity anomaly was isostatically corrected by computing the isostatic effect assuming a crustal thickness of 40 km, Bouguer densities of 2.67 gm/cc and 2.20 gm/cc for onshore and offshore respectively, and mantle density of 3.27 gm/cc. These parameters were determined using the method of Chapin (1996). Based on this model, the isostatic regional grid was calculated, utilising a GX from Northwest Geophysical Associates, and subtracted from the Bouguer gravity grid. Annotated contours use a base interval of 2 milligals.

Map 24 - First Vertical Derivative of the Isostatically-corrected Bouguer Gravity Anomaly Image With Shaded Relief

The grid of the first vertical derivative of the isostatically-corrected Bouguer gravity anomaly was prepared by applying a first vertical derivative filter in the frequency-domain. Colour break levels are set at variable intervals as modified from an equal-area colour distribution. Shaded relief illumination is applied from the north at a 45º inclination to the horizon.

Map 25 - First Vertical Derivative of the Reduction-to-the-Pole of the Total Magnetic Field Anomaly Image With Shaded Relief

The grid of the first vertical derivative of the reduction-to-the-pole of the total magnetic field anomaly was prepared by applying a first vertical derivative filter in the frequency-domain. Colour break levels are set at variable intervals as modified from an equal-area colour distribution. Shaded relief illumination is applied from the north at a 45º inclination to the horizon.

Map 26 - Compu-Drape™ of the Reduction-to-the-Pole of the Total Magnetic Field Anomaly Image With Shaded Relief

The grid of the reduction-to-the-pole of the total magnetic field anomaly was prepared by applying a pole-reduction filter in the frequency-domain. Compu-drape™ (Paterson et al., 1990) was then applied to compute the pole-reduced magnetic field on the sea floor/ground surface, through variable downward continuation. The

magnetic field is downward continued to a series of parallel surfaces that bracket the topographic surface, and then interpolated to that surface itself. Colour break levels are set at variable intervals as modified from an equal-area colour distribution. Shaded relief illumination is applied from the north at a 45º inclination to the horizon.

Compu-drape™ is a trademark of Paterson, Grant & Watson Limited.

Map 27 - Source Edge Detection from the Reduction-to-the-Pole of the Total Magnetic Field Anomaly

The grid of the horizontal gradient of the reduction-to-the-pole of the total magnetic field anomaly was prepared by computing the gradient amplitude as $[(dF/dx)^2 + (dF/dy)^2]^{1/2}$ in the space-domain. The local peaks in the horizontal gradient were then located, and those with a peak in at least two of four directions (N-S, NE-SW, E-W, SE-NW) were retained (Blakely and Simpson, 1986). They are plotted as strike-dip symbols, with the strike oriented perpendicular to the direction of maximum gradient in the original pole-reduced magnetic field, and the dip oriented "down-gradient". These symbols trace the location of contacts that exhibit a magnetic susceptibility contrast, assuming they have a steep dip. The dip symbol points away from the magnetic source.

Map 28 - Source Edge Detection from the Isostatically-corrected Bouguer Gravity Anomaly

The grid of the horizontal gradient of the isostatically-corrected Bouguer gravity anomaly was prepared by computing the gradient amplitude as $[(dF/dx)^2 + (dF/dy)^2]^{1/2}$ in the space-domain. The local peaks in the horizontal gradient were then located, and those with a peak in at least two of four directions (N-S, NE-SW, E-W, SE-NW) were retained (Blakely and Simpson, 1986). They are plotted as strike-dip symbols, with the strike oriented perpendicular to the direction of maximum gradient in the original pole-reduced magnetic field, and the dip oriented "down-gradient". These symbols trace the location of contacts that exhibit a density contrast, assuming they have a steep dip. The dip symbol points away from the gravity source.

Map 29 - Magnetic Anomaly Source Depth Using Source Parameter Imaging™

Source Parameter Imaging™ (Thurston and Smith, 1997) was applied the total magnetic field anomaly grid to determine the depths to magnetic sources, assuming a step-source model. The method utilises the horizontal and vertical gradients to determine the "local wavenumber" that is inversely proportional to depth. Only those solutions determined

to occur over a step-source are retained. The solutions are presented as circles with colour scaled to depth below ground/sea surface, with colour break levels set at variable intervals as modified from an equal-area colour distribution. The circle diameters are also scaled to reflect depth (4000m/mm).

Source Parameter Imaging™ is a trademark of Geoterrex-Dighem.

4. Magnetic and Gravity Interpretation

The enhanced processing, presentation and subsequent interpretation of the potential field maps in the Porcupine Basin area have been successful in generating a regional overview of a number of tectonic features, basin outlines with internal basin structure, and the location of regional faults. In addition, new igneous intrusive centres have been detected and the extent of volcanic sills and/or flows within the sedimentary column has been outlined.

The current interpretation has focused on large-scale features; however, at the presentation scale of 1:1,000,000 and with a dataset grid-cell size of 2 km (2 mm at map scale) a more detailed structural interpretation may be undertaken.

Earlier interpretation studies (P.A.D., 1999 and P.E.S.G.B., 1997) were consulted as part of the present work and, where possible, the previously used nomenclature has been incorporated. Structural features, igneous centres and vdcanic flows noted on the earlier studies were only incorporated if they were verified by the interpretation of the current potential field data.

In particular, we note the following features that have been outlined from the two previous studies noted above:

i) Basin Outlines – Clare, South Porcupine, North Porcupine, Tertiary, Canice, South Bróna, North Bróna, Pádraig, Macdara, Fursa, Colm, Cillian, Slyne, Fastnet, Little Sole, Melville Sub-Basin and Haig-Fras.
ii) Structural Elements – Iapetus Suture (7º W to 11ºW), Porthmarnock Horst, Merlin Ridge, Goban Graben, King Arthur Ridge, Variscan Front, Fastnet Ridge, Labadie Bank.
iii) Igneous Centres previously identified – Drol, Donn and Brendan

The interpretative work of the present study has focused on the area west of 10° W, extending from the coast of Ireland to the edge of the Rockall Basin.

The composite magnetic and gravity interpretation is presented on Map 1 (Figure 3).

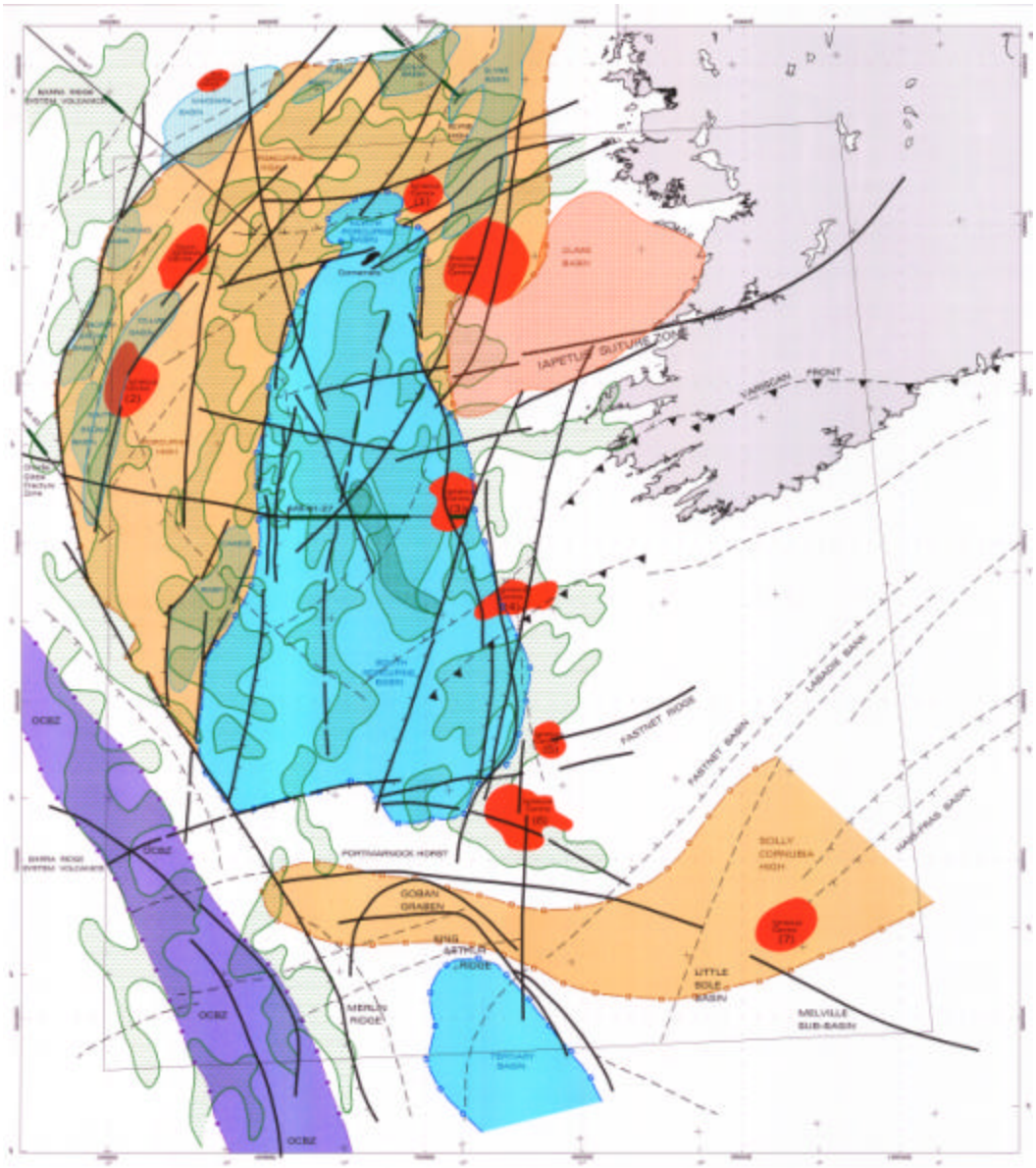

Figure 3 Magnetic and gravity interpretation (see Figure 3a for Legend).

In the interpretive process, all of the processed maps were consulted, with the following suite of maps proving to be the most useful in delineating the large-scale regional elements and igneous activity:

- First Vertical Derivative of the RTP Magnetic Field Image Map 25

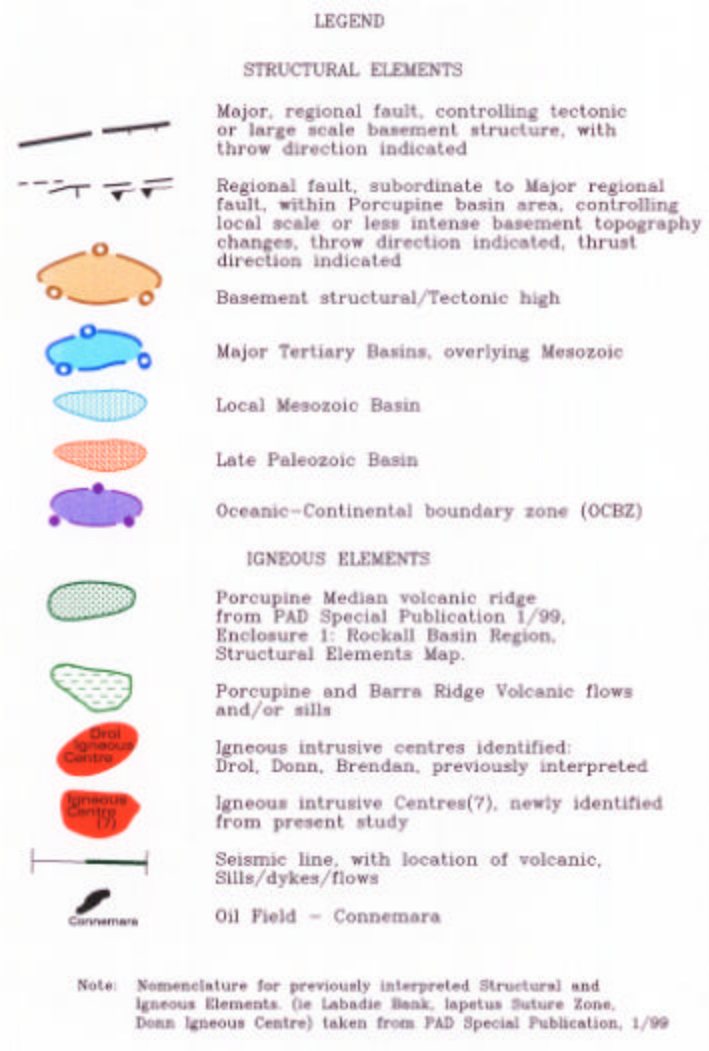

Figure 3a *Legend for magnetic and gravity interpretation (Figures 3,4 and 5).*

- Analytic Signal of TMI with Contours Map 18
- Horizontal Gradient of Isostatically-corrected Bouguer Gravity Anomaly Image Map 9
- Residual of the Isostatically-corrected Bouguer Gravity Image Map 10
- Compu-Drape™ of the RTP of the TMI Anomaly Image Map 26
- Source Edge Detection for RTP of TMI Anomaly Field Map 27

- Source Edge Detection of Isostatically-corrected Bouguer Anomaly Map 28

As aids in determining the movement, or throw, across regional faults and in outlining the extent of deep basins and shallow volcanics, the following semi-quantitative maps have proven to be very useful:

- Focused Magnetic Euler Solutions for Structural Index of 0.0 (contact) Map 21-1
- Focused Magnetic Euler Solutions for Structural Index 1.0 (sill/dyke) Map 21-2
- Gravity Euler Solutions for Structural Index of 0 (contact or step) Map 11

The discussion of the interpretation will be subdivided into three categories: Tectonic Features, Basins and Faults, and Igneous Activity.

a) **Tectonic Features**

Three major tectonic features that have deep-seated effects on the continental crust have been interpreted, the Iapetus Suture Zone, the Charlie Gibbs Fracture Zone Extension and the Oceanic-Continental Boundary Zone (OCBZ).

i) *Charlie Gibbs Fracture Zone Extension*

The interpretation of the processed magnetics (Maps 25, 26) and the gravity (Map 24) indicate a sharp E-W break in the regional N-S anomaly trends corresponding to a major E-W fault crossing the Porcupine High and ending in the western portion of the South Porcupine Basin in the region of 51° 30'N. Earlier studies (P.A.D., 1999) have indicated an eastern extension of this oceanic fracture to 17° 50'W, whereas the current analysis extends the fracture as far east as 13° W and indicates probable tectonics effects into the overlying crust. The left lateral movement evident within the oceanic crust to the west is not as apparent within the overlying crust in the Porcupine High region.

ii) *Iapetus Suture Zone*

The Caledonian age Iapetus Suture Zone observed onshore, exhibits strong evidence for an offshore extension as far as the western edge of the South Porcupine Basin. The present study of the First Vertical Derivative of the Bouguer gravity (Map 24) and the

Analytic Signal of the TMI (Map 18) clearly illustrate E-W to ENE-WSW anomaly pattern disruptions and/or terminations extending along the southern edge of the Clare Basin and traversing the South Porcupine Basin. In particular, the processed magnetics (Maps 25 and 18) indicate dextral wrench faulting, associated with the Iapetus Suture Zone, similar to that observed on-shore in the Irish Midlands.

iii) *Oceanic-Continental Boundary Zone OCBZ*

The OCBZ crosses the study area in the southwest corner, striking NNW from 14° W, 48° N. The OCBZ is bounded on the east by a dominant NNW-striking fault, seen on all processed maps and particularly on the first vertical derivative gravity (Map 24). The zone appears as a 50 km wide trend, stepping down from thinned continental crust to the east, to oceanic crust in the west. Both magnetic (Map 21-2) and gravity (Map 11) Euler solution plots, where not overprinted by volcanics, indicate a fault controlled increase in depth to the Porcupine Abyssal Plain to the SSW.

b) **Basins and Faults**

Interpretation of the processed potential field data has assisted in defining the limits of the two major sedimentary basins (Figure 4), the South Porcupine Basin and the Tertiary Basin, or Porcupine Seabright Basin. Both magnetic and gravity interpretations indicate a northern limit to the South Porcupine Basin at approximately 53° 10'N, the basin being terminated/uplifted by major E-W to ENE-WSW faults. The southern limit of the South Porcupine Basin occurs across major E-W to ENE-WSW faults (Maps 24,19 and 18) at approximately 50°N.

The Tertiary Basin exhibits a change in basement strike direction from predominately N-S (South Porcupine Basin) to the OCBZ NNW-SSE trend, as exhibited on the derivative gravity map (Map 24) and the residual magnetics (Map 17). The two basins are separated by the interpreted east-west striking Porthmarnock/Scilly-Cornubia High. Both magnetic and gravity Euler depth calculations (Maps 11 and 21-1) indicate a depth of 3km, or less, over this High, relative to magnetic/gravity basement depths of more than 10 km in the neighbouring South Porcupine and Tertiary Basins.

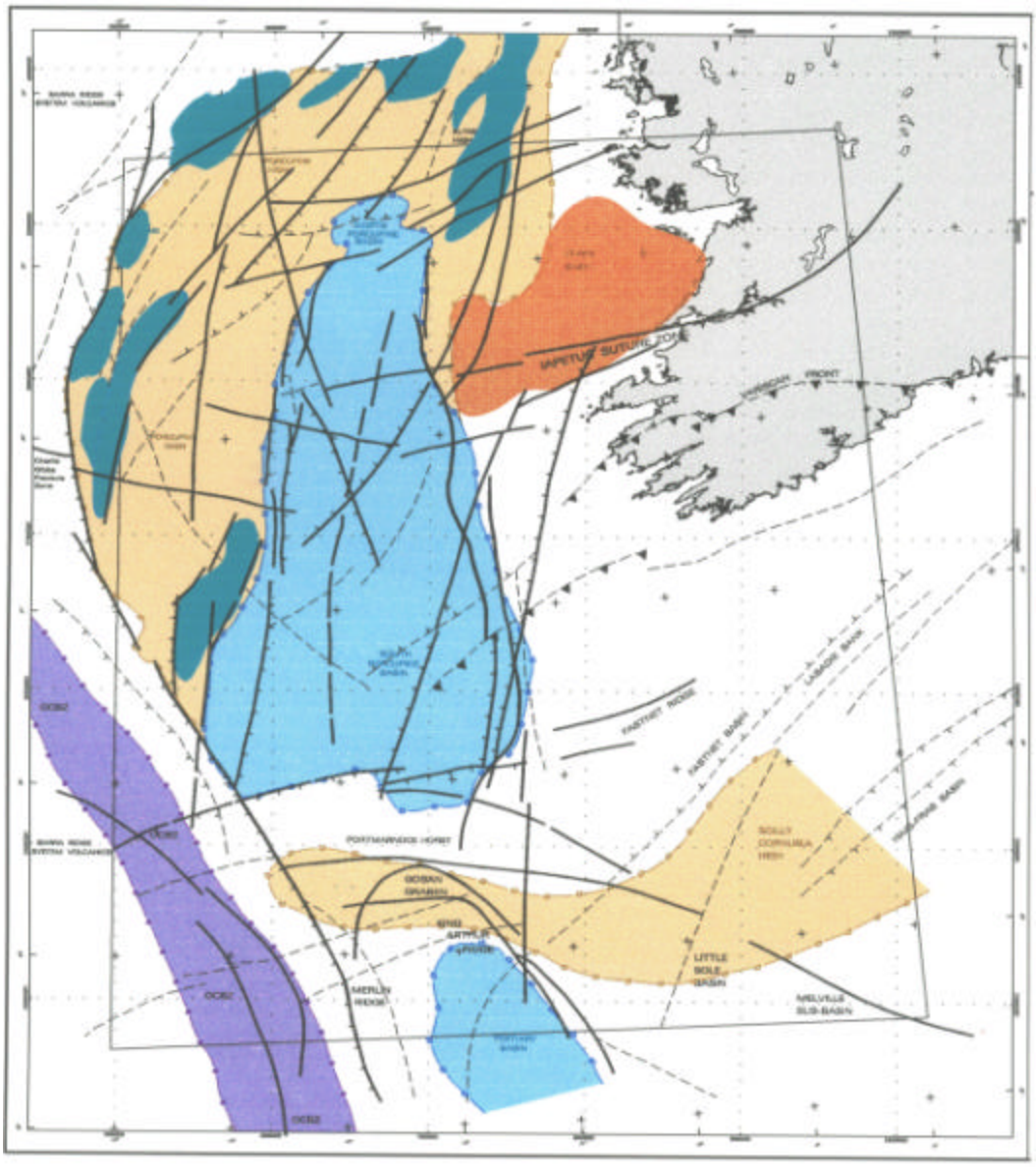

Figure 4 *Structural elements from the magnetic and gravity interpretation (see Figure 3a for Legend).*

The interpreted east-west striking high between the South Porcupine and Tertiary Basins is severely disrupted by the regional E-W faults. Shallow and/or local features associated with the high (i.e. Goban Graben and King Arthur Ridge) have been identified from previous studies and are included on the present interpretation map.

A number of the smaller Late Palaeozoic (Clare), Mesozoic (Pádraig, Macdara), and Tertiary (Colm, Cillian) basins all exhibit noticeable gravity/magnetic signatures. In particular, the derivative gravity (Map 24) is generally low over the basins.

Where not overprinted by igneous or volcanics patterns, the magnetics also generally reflects a quieter, lower magnitude signature (Clare, Macdara and Colm) over the basins.

Numerous regional faults have been noted on the interpretation map. Each of these features has been interpreted by joint analysis/inspection of vertical derivative and analytic signal magnetics and the residual and horizontal gradient of the gravity. In all cases, these faults effect and/or control basement topography, as interpreted from the gravity and magnetic Euler solutions. In many cases, the faults appear to penetrate the volcanic units and may, in some cases, form conduits or limits to the flows.

The South Porcupine Basin exhibits a more complex regional structural pattern than has been previously interpreted. The major N-S (340° to 20°) faults limiting the eastern and western boundaries of the basin have been interpreted from disruptions, terminations and offsets in the processed derivative magnetic and gravity patterns. Two "new" fault trends have been interpreted within the basin (Figure 4); the first being a NE to NNE trend represented by four major faults traversing the basin in a stepwise fashion beginning at the northern edge of the Median Volcanic Ridge and extending to the southeastern corner of the basin in the region of Igneous Centres 5 and 6. The second major trend strikes approximately E-W across the middle of the Basin between 51° 30´N and 52° 30´N. As noted previously, these three E-W faults are associated with the Iapetus Suture Zone and the eastern extension of the Charlie Gibbs Fracture Zone.

c) **<u>Igneous Activity, including intrusions and volcanic flows</u>**
Igneous activity in the South Porcupine Basin area has been indicated from the results of previous seismic and potential field studies (P.A.D., 1999). The interpretation of the current processed magnetic and gravity data has verified a number of these suspected intrusive features and has indicated more active intrusive activity around the faulted edges of the South Porcupine Basin (Figure 5). As well, a much more extensive development of Cretaceous and late Tertiary volcanism within the South Porcupine Basin and to the west on the Porcupine High, has been interpreted. The flows associated with the early Cretaceous age Barra Ridge volcanics have been interpreted to extend onto the OCBZ in the south and up to the edge of the Mesozoic basins on the northwestern edge of the Porcupine High.

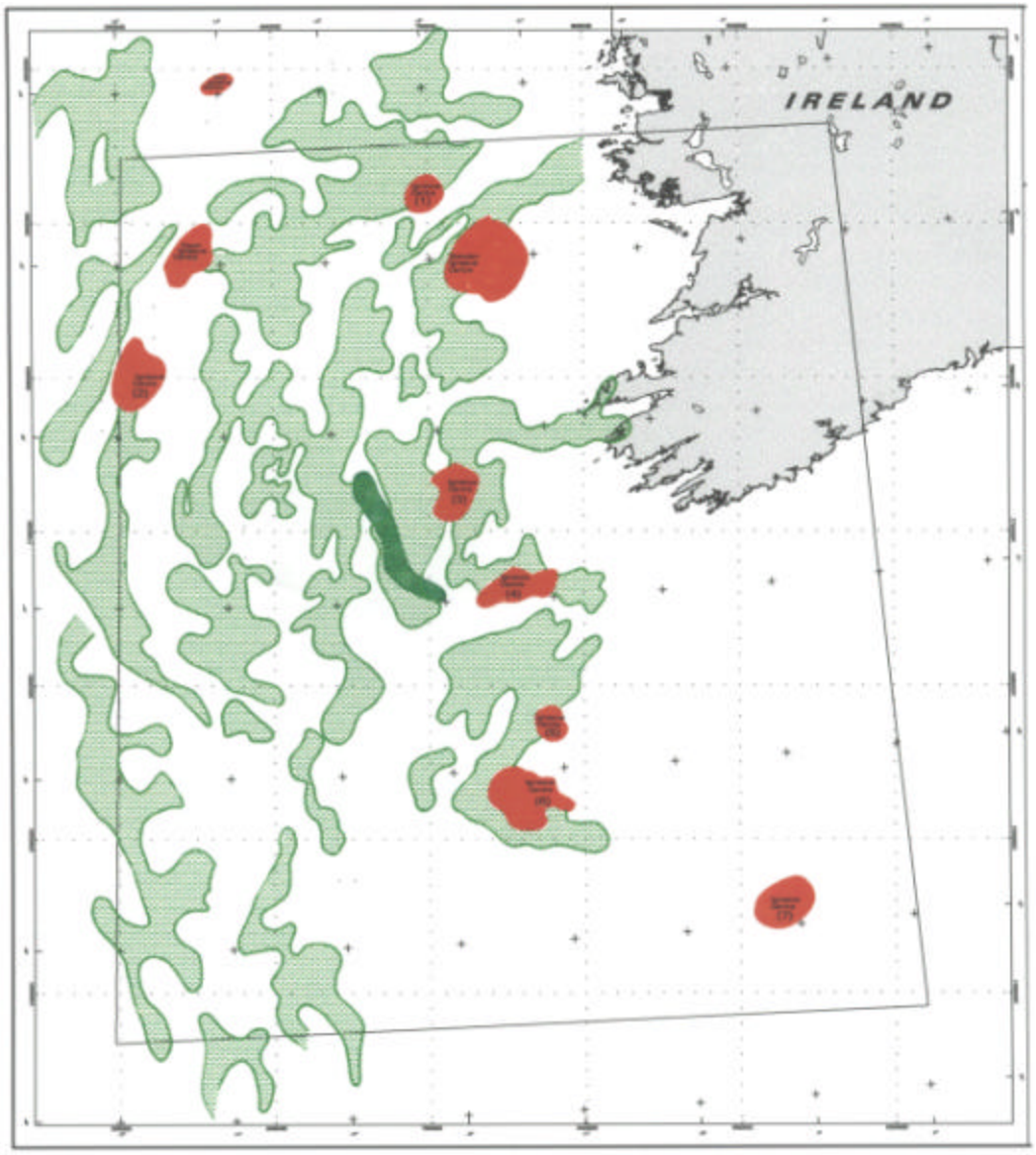

Figure 5 Igneous elements from the magnetic and gravity interpretation (see Figure 3a for Legend).

ci) **Igneous Activity: Intrusive Igneous Centres**

The three previously noted Igneous Centres (Brendan, Donn and Drol) all exhibit positive (i.e. shallow) response on the calculated magnetic Euler Solutions (Map 21-2), with the exception of the eastern one-third of the Brendan Intrusive, which appears to be down faulted to east, across a N-S regional fault at the edge of the Clare Basin. The analytic signal of the TMI (Map 18) indicates a positive magnetic response over Brendan and Donn and an indistinct signature over the smaller Drol Intrusive.

Seven new intrusive bodies have been interpreted in the current study. Five of these igneous centres lie along the eastern edge of the South Porcupine Basin and are associated with, and possibly are contemporaneous with, N-S, NNE-SSW boundary faults and with the northern ENE boundary faults. All of these igneous centres exhibit anomalous responses on the analytic signal map and all intrude the lower to middle units of the basin sediments, as indicated by the shallow calculated depths of 5000 m, or less, on both the magnetic and, to a lesser extent, gravity Euler solution plots (Maps 21-2 and 11). Igneous Centres 4, 5 and 6 exhibit strong positive, circular to oval magnetic signatures, (Map 18), whereas Centres 3 and 1 appear as "zoned" intrusions, with positive magnetic margins surrounding by a lower susceptibility core. The new off-basin Centres, 2 and 7 also both exhibit strong positive circular magnetic responses (Map 18) and relatively shallow depths (Centre 2 is 7 km, or less, on the edge of the Porcupine High and Centre 7 intrudes to a depth of 3 km or less on the edge of the Haig-Fras Basin).

The presence of six igneous centres correlating with regional N-S faults along the eastern edge of the South Porcupine Basin indicates active tectonism and fault rejuvenation into late Cretaceous and probably early Tertiary time.

cii) **Igneous Activity: Volcanic Flows**

The limited exposure of extrusive igneous rocks noted from the earlier seismic interpretation of profile MS-81-27 (Line N, Enclosure 2, P.A.D., 1999) was a one-line sample of a much larger expanse of volcanic rock that covers much of the South Porcupine Basin and the Porcupine High to the west. The pervasive extent of the Cretaceous age volcanic (basalt) flows is exhibited to a greater or lesser extent, on all of the processed potential field maps. In particular, we note three processing techniques that highlight the extent and location of the volcanism:

Map 18 – *Analytic Signal of TMI*

The majority of the positive, non-intrusive, analytic signal anomalies represent volcanic (basalt) flows at various levels within the Cretaceous-Tertiary stratigraphy. The shallowest, and probably youngest, sequences of flows occur along the eastern and western faulted boundaries of the South Porcupine Basin. The fault-related intrusives along the eastern basin edge were probably the sources for the shallow flows.

As noted on the seismic interpretation, the analytic signal magnetic signature indicates more deeply buried, possibly older, flows in the centre of the basin.

Map 24 – *First Vertical Derivative, Bouguer Gravity*
In general, the positive broad linear, N-S striking, continuous gravity anomalies on the derivative map correlate with zones of volcanic flows. This correlation of anomalous volcanic gravity and magnetic response is well illustrated in a N-S striking zone extending almost the whole length of the South Porcupine Basin at approximately 12° 30´W. Earlier studies have concluded that the Porcupine Median Volcanic Ridge (noted on the present interpretation map 1) was a strike-limited NW-SE feature. The current results indicate a more extensive 300 km N-S ridge, or mid basin fracture, that may be the volcanic/igneous conduit and that this conduit is probably associated with a regional mid-basin N-S fault that has been rejuvenated throughout Cretaceous and Tertiary time.

Maps 11, 21-1 and 21-2 – *Euler Solutions, Gravity and Magnetics*
The Euler depth solutions for magnetic anomalies within a basin devoid of igneous activity will reflect, in a general sense, the basement topography of the basin. This can be seen, in the present study, for the Palaeozoic Clare Basin (Maps 11 and 21-2), particularly west of 10°W. Focused magnetic Euler solutions yield average depths-to-basement of 8 km to 12 km, with a deepening to the south, to approximately 14 km, across the Iapetus Suture. Similar values are evident on the Gravity Euler Solutions (Map 11), ranging from 8 km to 16 km.

Within the South Porcupine Basin, both gravity and magnetic Euler depth calculations reflect the presence of basement sources as well as volcanic flows within the sediments. Along the western edge of the South Porcupine Basin, shallow magnetic depths (5 km or less) correlate with the interpreted volcanics. The central ridge volcanics, associated with the major N-S fault at 12° 30´W exhibit much deeper depths on the magnetics (10 km or greater) and also for the calculated gravity depths (12 km or greater), indicating a much deeper volcanic source. The potential field calculations agree, in a general sense, with the "deep-source" igneous body (approximate depth of 8 to 10 km) noted on the seismic line MS-81-27.

5. Conclusions

The enhanced processing, presentation and interpretation of the potential field data has provided significant new input to the regional framework of the Porcupine Basin area. In particular, new regional faults, igneous centres and volcanic flow regions have been delineated as a result of the current study. More detailed interpretation if the gravity and magnetic data will provide important input to the local interpretation of seismic lines and will help to tie the seismic interpretation to the regional framework. Future modelling of specific features using the gravity and magnetic data will lend further verification to interpretive seismic results.

References

ARK Geophysics Ltd., 2000, Compilation Report – Porcupine Basin Potential Field Study, Porcupine Studies Group Secretariat.

Blakely, Richard J., and Simpson, R. W., 1986, Approximating edges of source bodies from magnetic or gravity anomalies (short note), Geophysics, v. 51, p. 1494-1498.

Chapin, David A., 1996, A deterministic approach toward isostatic gravity residuals – A case study from South America, Geophysics, v. 61, p. 1022-1033.

Paterson, Norman R., Reford, S. W. and Kwan, K. C. H., 1990, Continuation of magnetic data between arbitrary surfaces: Advances and applications, Annual Meeting Abstracts, Society Of Exploration Geophysicists, p. 666-669.

Petroleum Affairs Division (P.A.D.), 1999, Irish Rockall Basin region – a standard structural nomenclature system, Special Publication 1/99, Dublin, Ireland.

Petroleum Exploration Society of Great Britain (P.E.S.G.B.), 1997, Structural framework of the North Sea and Atlantic Margin, 1:1 500 000 scale map.

Reid, Alan B., Allsop, J. M., Granser, H., Millett, A. J. and Somerton, I. W., 1990, Magnetic interpretation in three dimensions using Euler deconvolution, Geophysics, v. 55, p. 80-91.

Thurston, Jeffrey B., and Smith, R. S., 1997, Automatic conversion of magnetic data to depth, dip, and susceptibility contrast using the SPI™ method, Geophysics, v. 62, p. 807-813.